Gradual wavelet reconstruction of the velocity increments for turbulent wakes

C. J. Keylock, R. Stresing, and J. Peinke

Citation: Physics of Fluids (1994-present) **27**, 025104 (2015); doi: 10.1063/1.4907740

View online: http://dx.doi.org/10.1063/1.4907740

View Table of Contents: http://scitation.aip.org/content/aip/journal/pof2/27/2?ver=pdfcov

Published by the AIP Publishing

PHYSICS OF FLUIDS **27**, 025104 (2015)

Gradual wavelet reconstruction of the velocity increments for turbulent wakes

C. J. Keylock,[1,a)] R. Stresing,[2] and J. Peinke[2,b)]
[1]*Sheffield Fluid Mechanics Group and Department of Civil and Structural Engineering, University of Sheffield, Mappin Street, Sheffield S1 3JD, United Kingdom*
[2]*Institute of Physics, University of Oldenburg, 26111 Oldenburg, Germany*

(Received 25 June 2014; accepted 26 January 2015; published online 10 February 2015)

This work explores the properties of the velocity increment distributions for wakes of contrasting local Reynolds number and nature of generation (a cylinder wake and a multiscale-forced case, respectively). It makes use of a technique called gradual wavelet reconstruction (GWR) to generate constrained randomizations of the original data, the nature of which is a function of a parameter, ϑ. This controls the proportion of the energy between the Markov-Einstein length (~0.8 Taylor scales) and integral scale that is fixed in place in the synthetic data. The properties of the increments for these synthetic data are then compared to the original data as a function of ϑ. We write a Fokker-Planck equation for the evolution of the velocity increments as a function of spatial scale, r, and, in line with previous work, expand the drift and diffusion terms in terms up to fourth order in the increments and find no terms are relevant beyond the quadratic terms. Only the linear contribution to the expansion of the drift coefficient is non-zero and it exhibits a consistent scaling with ϑ for different flows above a low threshold. For the diffusion coefficient, we find a local Reynolds number independence in the relation between the constant term and ϑ for the multiscale-forced wakes. This term characterizes small scale structure and can be contrasted with the results for the Kolmogorov capacity of the zero-crossings of the velocity signals, which measures structure over all scales and clearly distinguishes between the types of forcing. Using GWR shows that results for the linear and quadratic terms in the expansion of the diffusion coefficient are significant, providing a new means for identifying intermittency and anomalous scaling in turbulence datasets. All our data showed a similar scaling behavior for these parameters irrespective of forcing type or Reynolds number, indicating a degree of universality to the anomalous scaling of turbulence. Hence, these terms are a useful metric for testing the efficacy of synthetic turbulence generation schemes used in large eddy simulation, and we also discuss the implications of our approach for reduced order modeling of the Navier-Stokes equations. [http://dx.doi.org/10.1063/1.4907740]

I. INTRODUCTION

Progress on the understanding of a stochastic description of turbulence since Kolmogorov[1] (K41) has focused on Landau's objection and the subsequent realisation that corrections to K41[2] imply that turbulence is intermittent.[3] However, as yet, no postulated model for intermittency has received universal acceptance or has been derived directly from the Navier-Stokes equations at high Reynolds number. Instead, a variety of phenomenological models have been proposed[2–5] (see Dowker and Ohkitani[6] for a recent comparative analysis) and exactly how intermittency may be

a)Electronic mail: c.keylock@sheffield.ac.uk
b)peinke@uni-oldenburg.de

characterized is an open question, as is the manner in which it depends on the large scale forcing of the flow.[7]

Classical theory is predicated on an assumed forcing at a single, large scale. Energy transfer towards viscous scales self-organizes into a scaling region with a −5/3 slope. In K41 and elsewhere, no dependence on the larger scales is assumed, although there are studies that interrogate this assumption,[7,8] as well as those studying the dependence between scales in general through triadic interactions.[9] In the last decade, there has been a concerted effort to understand the implications of forcing the flow at multiple scales.[10–14] This work has focused primarily on characterizing the dissipation properties of freely decaying, multiscale-forced turbulence, with connections noted to notions of exponential decay.[15,16] In addition, numerical simulation has elucidated the mechanisms by which multiscale forcing operates[17,18] and recent work has also begun to explore the implications of multiscale forcing for pipe and boundary-layer flows.[19,20] In a recent study of the conditional probability distribution functions for the velocity increments of jets, cylinder wakes, and multiscale-forced flows,[21] it was found that the statistics for the velocity increments were independent of Taylor Reynolds number, Re_λ, for the multiscale-forced cases. As a consequence, turbulence decay for these flows differed from that classically assumed in the Richardson-Kolmogorov view of turbulence.[1,22]

The aim of this paper is to study the conditional velocity increment distribution functions and thus, intermittency of jet and fractal-generated turbulence using a controlled randomization technique (termed Gradual Wavelet Reconstruction (GWR)[23]). Hence, in the strongly randomized synthetic datasets, we try to destroy the properties of the turbulence. We then generate other randomizations that gradually recover the properties of the original series. In this way, we can use the synthetic data as null models to explore hypotheses regarding the effect that the forcing has on the nature of turbulence. Section II of this paper explains the technique used for analysing the increment statistics. We then explain the randomization method, before examining the properties of the real data relative to the synthetic realizations, and the scaling of these results.

II. ANALYZING VELOCITY INCREMENTS

A. Structure function and multifractal approaches

It is common in turbulence to analyze intermittency using longitudinal structure functions,[24] which are the moments of the probability distribution function (PDF) of the velocity increments, $p[\xi(r)]$, where $\xi(r) = u(x+r) - u(x)$. The structure function of order n is given by $S_n = \langle \xi(r)^n \rangle$ and the non-intermittent K41 theory gives a relation between $\log r$ and $\log S_n$ with a constant slope of $\zeta = \frac{n}{3}$. Extensions to this work have characterised the spectrum of hypothesised singularities in the flow using a multifractal analysis where, classically, one uses a Legendre transform to determine the sets, $\mathbf{S}_{\alpha_x}$, with a given Hölder exponent, α_x, in the flow.[25,26] The singularity spectrum, $D(\alpha_x)$, is then the set of values for α_x for which $\mathbf{S}_{\alpha_x}$ is not empty. The Frisch-Parisi conjecture states that

$$D(\alpha_x) = \min_n(\alpha_x n - S_n + 1). \tag{1}$$

Hence, the structure function and multifractal approaches may be related explicitly and the latter is also closely related to the notion of the Kolmogorov capacity[27] (the scaling of the zero-crossings), which we employ towards the end of this paper.

This paper focuses on the longitudinal velocity increments and, as such, follows previous work that has adopted the Fokker-Planck approach to describing the evolution of turbulence structure.[28,29] However, the flows considered in this paper are anisotropic, and to help characterize the dynamics in this situation, longitudinal structure function analysis is sometimes complemented by a consideration of transverse structure functions.[30,31] Differences have been observed in their scaling, with some authors reporting greater intermittency for the transverse structure functions,[32] and others the opposite.[33] Hence, initial conditions, methodology (particularly identifying the scaling region), inhomogeneity, Reynolds number, and large scale anisotropy may all impact on the results. In a systematic exploration of these effects on jet flow, it was shown that large-scale anisotropy was the primary control,[34] although differences between the longitudinal and transverse structure functions

do not necessarily affect the dynamics of the cascade, which can be shown to belong to the same universality class concerning the hierarchical expression of intermittency despite differences in the exponents.[35] Hence, while an analysis of longitudinal increments may be complemented by a study of transverse increments in anisotropic flows, significant value remains in the analysis of the longitudinal increments, and the extension of the structure function approach to the full PDF of the increments adds an extra richness to analysis.

B. Fokker-Planck equation for the velocity increments

The use of a Fokker-Planck equation to describe the evolution of the PDF of the velocity increments as a function of r was pioneered in several papers fifteen years ago.[28,29,36] For scales greater than the Markov-Einstein coherence length l_{EM}, which is $\sim 0.8\lambda$,[37] experimental observations[21,29] show that the increment statistics have the Markov property across scales,

$$p(\xi_j|\xi_{j+1}) = p(\xi_j|\xi_{j+1},\xi_{j+2},\ldots,\xi_{j+R}), \tag{2}$$

where $\xi_j \equiv \xi(r_j)$ and R is the number of scales, each separated from the other by at least l_{EM}. (In fact, defining $\Delta r = r_{j-1} - r_j$, then l_{EM} is the smallest Δr for which Eq. (2) holds.)

Given that the Markov property holds, this method may then be used to evaluate the joint distribution function for $p(\xi_{1,2,\ldots,R}) \equiv p(\xi_1,\xi_2,\ldots,\xi_R)$ from the product of the conditional distribution functions. The stochastic process for the conditional PDFs is given by a Kramers-Moyal expansion, and Pawula's theorem states that if the fourth order Kramers-Moyal coefficient is zero, the expansion truncates at the second term to give a Fokker-Planck equation[28,38]

$$-r_j\frac{\partial}{\partial r}p(\xi_j|\xi_0) = -\frac{\partial}{\partial \xi}[D^{(1)}(\xi,r)p(\xi_j|\xi_0)] + \frac{\partial^2}{\partial \xi^2}[D^{(2)}(\xi,r)p(\xi_j|\xi_0)], \tag{3}$$

where $r_j < r_0$. Hence, the evolution of the PDF for the conditional increments is governed by drift, $D^{(1)}$, and diffusion, $D^{(2)}$, coefficients in accord with an advective-diffusive stochastic process generated by a Langevin equation

$$-r_j\frac{\partial}{\partial r}\xi_j(r) = D^{(1)}(\xi,r) + \sqrt{D^{(2)}(\xi,r)}f(r), \tag{4}$$

where $f(r)$ is a δ-correlated Gaussian white noise. Following previous work,[29] we estimate the coefficients by

$$D^{(k)}(\xi,r) = \lim_{\Delta r\to 0}\frac{r}{k!\Delta r} \times \int_{-\infty}^{+\infty}(\xi^* - \xi)^k p[\xi^*(r-\Delta r)|\xi(r)]d\xi^*, \tag{5}$$

where ξ^* is the dummy integration variable. We then write the drift and diffusion terms as a function of ξ, treating terms up to fourth order,

$$\begin{aligned} D^{(1)}(\xi,r) &= d_{10}(r) - d_{11}(r)\xi + d_{12}(r)\xi^2 - d_{13}(r)\xi^3 + d_{14}(r)\xi^4, \\ D^{(2)}(\xi,r) &= d_{20}(r) - d_{21}(r)\xi + d_{22}(r)\xi^2 - d_{23}(r)\xi^3 + d_{24}(r)\xi^4. \end{aligned} \tag{6}$$

It has then been shown previously for experimental data[21,36] that the drift term can be simplified to a linear expression in ξ,

$$D^{(1)}(\xi,r) = -d_{11}(r)\xi, \tag{7}$$

and the diffusion term as a quadratic in ξ,

$$D^{(2)}(\xi,r) = d_{20}(r) - d_{21}(r)\xi + d_{22}(r)\xi^2. \tag{8}$$

We demonstrate that this is also the case for the data studied, here, below. Thus, we emphasize that our use of this framework is to provide a more complete examination of the velocity increment distribution than a study of the moments. While our framework may be used for modeling purposes,[39] it is used here to study the properties of turbulence datasets (in a similar way to work examining the form of the intermittency in measured datasets[40]). Hence, the intention is not to inform a reduced order model for the dynamics,[41,42] although at the end of the paper, we consider the implications of our work for such an approach.

C. Structure functions and the Fokker-Planck approach

The PDF approach may be linked explicitly to classical tools for studying turbulence.[1,2,24] More specifically, if only d_{11} was non-zero, one would obtain classical Kolmogorov-like linear scaling of the structure functions as a function of moment order. Consequently, the terms associated with the expansion of $D^{(2)}$ contain information on intermittency and anomalous scaling. The quadratic term d_{22} corresponds to the fluctuations expressed as a multiplicative noise, a phenomenon incorporated into the log-normal model (K62).[2] The term d_{20} is then the departure from K62 responsible for the quadratic tip of the increment PDFs for small r.[28] This can be made explicit by considering a simpler form for the drift and diffusion coefficients than is actually needed,

$$D^{(k)}(\xi,r) = d_k\xi^k. \tag{9}$$

From the Kramer-Moyal expansion and the definition of the structure function of order n, $S_n = \langle \xi^n \rangle$, one can write[29]

$$-r\frac{\partial}{\partial r}S_n(r) = \sum_{k=1}^{n}\frac{n!}{(n-k)!}d_k S_n(r) \tag{10}$$

leading to scaling exponents

$$\zeta_n = -\sum_{k=1}^{n}\frac{n!}{(n-k)!}d_k \tag{11}$$

meaning that for $\zeta_3 = 1$ and no intermittency, we obtain $d_1 = -\frac{1}{3}$, while $d_1 = -0.39$ and $d_2 = 0.026$ are consistent with the K62 model.

D. Past work using the Fokker-Planck approach

Stresing and co-workers examined the increment statistics for free jets, wakes, and flows forced by a fractal square grid using the Fokker-Planck framework set out above.[21] While d_{11} exhibited a similar r dependence for different flows, with no significant Re_λ dependence, d_{20} was found to depend on r and Re_λ for the jet data, but not the fractal wakes. Given the linear relation between d_{20} and r/λ, characterised by its slope d_{20}^*, it was shown that as Re_λ was varied from ~150 to ~800, d_{20}^* maintained a constant value of 0.08 for the fractal forced flows. In contrast, it varied from $d_{20}^* \sim 0.1$ at $Re_\lambda \sim 80$ to $d_{20}^* \sim 0.02$ at $Re_\lambda \sim 1000$ for free jet flows and from $d_{20}^* \sim 0.09$ at $Re_\lambda \sim 80$ to $d_{20}^* \sim 0.055$ at $Re_\lambda \sim 350$ for cylinder wake flows. The coefficients d_{21} and d_{22} for jet data have also been shown to exhibit a Re_λ dependence,[30] but no such relations were found with the fractal-forced flows.

Interesting behavior of the velocity increment distributions was also recently observed in a fractal-forced boundary layer wake.[20] Wakes were generated using four different fences at the same fence-height Reynolds number. As shown in Fig. 1, the increment distributions for the fractal-forced cases (gray lines) were very similar, with much broader distributions than for the single-scale forced cases, even though the former two fences differed in their porosity (which is usually deemed to be the primary control on wake structure behind fences) and the latter did not.

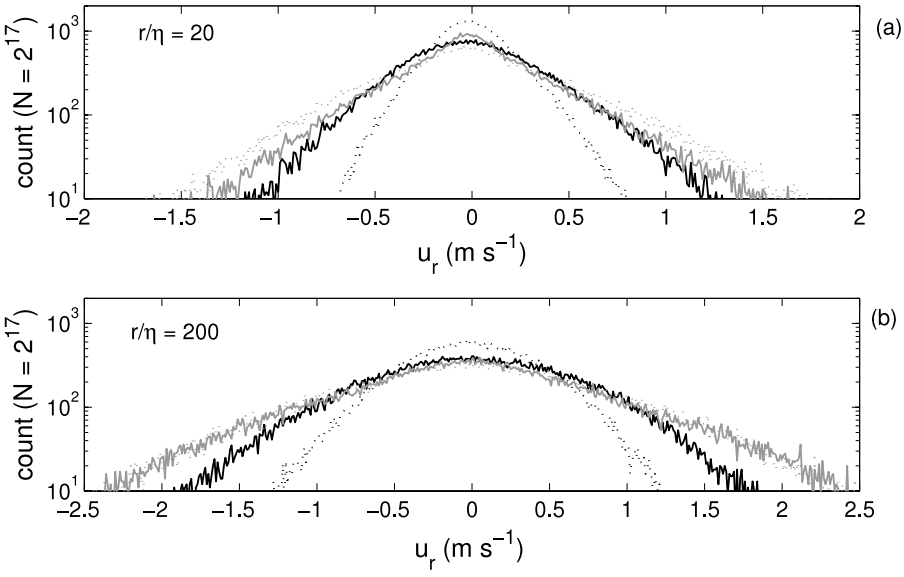

FIG. 1. Distribution functions of the velocity increments for two choices of r, non-dimensionalised by the Kolmogorov length, η, for wake flows 1.25 heights downstream of a porous fence immersed in a boundary layer.[20] The black lines are for two fences with a 50% porosity and forced at a single scale. The narrower distribution has a 5 mm gap between each element in the fence, while it is 10 mm for the broader distribution. The gray lines are for two fences with a multiscale, fractal forcing and 50% and 60% porosities.

III. GRADUAL WAVELET RECONSTRUCTION (GWR)

Hypothesis testing for nonlinearity using synthetic data is a well-known method in nonlinear dynamics.[43] For a selected significance level, $a = 2/(b + 1)$, and for a two-tailed statistical test, one generates a total of b synthetic, surrogate series. A metric of nonlinearity (e.g., increment skewness, correlation dimension, maximal Lyapunov exponent) is then applied to the original data and the surrogates. If the value of the metric for the original data is greater or less than that for all the surrogates, then a significant difference is deemed to exist.

Surrogate data generation methods such as the iterated amplitude adjusted Fourier transform (IAAFT)[44] are extensions of the phase randomization techniques that have been applied for analyzing the properties of turbulence datasets.[45] The IAAFT method is more suitable for formal hypothesis testing than a simple phase randomization because not only the Fourier amplitudes but also the values of the original data series are identical to those in the synthetic data. Gradual wavelet reconstruction[23] was introduced to study a rejection of the null hypothesis based on IAAFT surrogates (finding nonlinearity). By constraining the degree of phase randomization, surrogate series closer in nature to the original data are generated. Defining $\vartheta \in \{0, \ldots, 1\}$, where 0 is a phase-randomized IAAFT surrogate and 1 is the original data, GWR permits synthetic series to be generated for any choice of ϑ. As explained below in greater detail, ϑ is expressed in terms of the proportion of the time-frequency energy of the signal fixed in place in the synthetic series. For a nonlinear dataset (i.e., one where the null hypothesis has been rejected for a given metric of nonlinearity using IAAFT surrogates, or equivalently, for $\vartheta = 0$), we may then undertake a number of tests for increasing ϑ (using a Bonferroni corrected significance level) and identify the threshold, $\vartheta_{\text{thresh}}$, that delimits rejection ($\vartheta < \vartheta_{\text{thresh}}$) and acceptance ($\vartheta \geq \vartheta_{\text{thresh}}$) of the null hypothesis. For $\vartheta \geq \vartheta_{\text{thresh}}$, the surrogates and data are similar and the former may be considered legitimate realisations of the latter with respect to the metric of nonlinearity adopted. Thus, $\vartheta_{\text{thresh}}$ can be used to determine the degree of nonlinearity in two datasets, to measure the sensitivity of metrics of nonlinearity applied to turbulence time series,[23] or as the value for which to generate synthetic data that preserve the nonlinearity of a particular process.[46] Alternatively, synthetic velocity time series may be generated as a function of ϑ and used to form the inlet boundary conditions of eddy-resolving numerical simulations, highlighting any dependencies on the prescribed inlet condition.[47]

A. Generating synthetic data with GWR

GWR makes use of a Maximal Overlap Discrete Wavelet Transform (MODWT) to fix in place some of the temporal/spatial structure of the original data as a function of ϑ. The MODWT is a perfect choice because unlike the continuous wavelet transform, it is exactly reconstructible, meaning that we can recover a synthetic series from a set of wavelet coefficients by taking the inverse transform. The discrete wavelet transform (DWT) also has this property but is a decimated transform (the number of wavelet coefficients, $w_{j,k}$, varies as function of wavelet scale, j) and is restricted to the analysis of data series of length $N = 2^J$, where $J \in \mathbb{Z}$. The MODWT is undecimated and is not limited to data series where $\log N/\log J = 2$. Other advantages of this approach are given in the text by Percival and Walden[48] and the original GWR paper.[23] The Appendix briefly reviews the continuous, discrete, and MODWT wavelet methods.

A MODWT of a data series, $u(x)$ consisting of N velocity measurements, gives $J \times N$ detail coefficients, $w_{j,k}$, where $k = 1,\ldots,N$ and $j = 1,\ldots,J$, where J is the number of wavelet scales investigated. While this has been the way that GWR was used in the past (to randomize all frequencies in the data series), in this study, we constrain the frequency decomposition of the signal such that its lower limit corresponds to l_{EM} and J is set to an upper limit that is close to but includes the integral scale, L.

The basic idea in GWR is to then to randomize the $w_{j,k}$ at a given j using the IAAFT algorithm.[49] By preserving all the original values for the $w_{j,k}$, there is no change to the moments of the wavelet coefficients (whose variance at a given j is proportional to the Fourier energy at this frequency band). By preserving the periodicities in the wavelet coefficients, the resulting series is a potentially legitimate output from a wavelet transform at scale j. To couple our approach as closely as possible to Fourier-based methods, the definition of ϑ is based on the $w_{j,k}^2$ (which are stationary and zero-mean).[50] All $J \times N$ coefficients, $w_{j,k}^2$, are placed in an ordered set, $\mathbf{A}$ in descending rank order. If the total wavelet energy is $\sum_{i\in\mathbf{A}} w_i^2$, then for a selected value of ϑ, we seek a value g such that

$$\vartheta = \frac{\sum_{i\in\mathbf{A}}^{g} w_i^2}{\sum_{i\in\mathbf{A}} w_i^2}. \tag{12}$$

Thus, g is the smallest number of coefficients that fulfil the choice of ϑ. By prioritizing the largest magnitude coefficients, our method is in the spirit of wavelet denoising methods,[51] where the $|w_{j,k}|$ that fall below a threshold based on a Gaussian model for the coefficients at $j = 1$ are considered as noise and are set to zero. Using Eq. (12), we then define $\mathbf{F} \subseteq \mathbf{A}$ as the g length subset of fixed coefficients and return these to their original locations on the J by N wavelet plane indexed by j and k. We then return the unfixed coefficients, $\mathbf{F}^C$, to unique random positions along the time/space axis for their original value for j and perform a scale-by-scale randomization similar to the IAAFT but with the starting point that a subset of the wavelet coefficients is fixed rather than randomized.[50] Hence, in the lower limit of $\vartheta = 0$, no coefficients are fixed and we have a phase-randomized synthetic series similar to the IAAFT method, while at the upper limit $\vartheta = 1$, all coefficients are fixed in place and no randomization occurs. The inverse wavelet transform is then used to recover a data series.[23,50]

An alternative to GWR would be an additive phase noise approach.[52] Given a velocity signal, $u(x)$, with an associated phase spectrum, $\phi_u(k)$, that is a function of wave number, k, we may form a new phase spectrum: $\phi(k) = (1-\epsilon)\phi_u(k) + \epsilon\phi_R(k)$, where $0 \le \epsilon \le 1$ is a noise level and $\phi_R(k)$ is a uniformly distributed random variate over wavenumber. The primary advantage of GWR is that we can constrain the randomization to a specific range of scales, i.e., those between l_{EM} and L. It follows that we only define $\mathbf{A}$ and, thus, ϑ over this range of scales too. Another potential advantage of GWR is that it constrains the degree of variation in a particular subsection of a signal based on the extent to which the $w_{j,k}$ are fixed. Given the acceptance of the null hypothesis of no significant difference between original data and surrogate series at some choice for ϑ, but the rejection at a lower ϑ, this permits the components of the signal that are essential for preserving a particular property of the original data to be identified. In addition, the ability to constrain the values of the synthetic signal to those of the original is also advantageous for hypothesis testing.[43]

B. Use of GWR in this study

We generated synthetic series for $\vartheta \in \{0, 0.25, 0.4, 0.5, 0.6, 0.7, 0.8, 0.9\}$ for two wake datasets and two fractal grid datasets described in Sec. IV. Figure 2 provides a qualitative assessment of the way in which GWR works for four choices of ϑ. It is clear from the top panel that $\vartheta = 0$ is generating a phase-randomized signal (gray line) with no alignment with the original data (black line). As $\vartheta \to 1$, surrogates converge on the original data. Because there is higher energy at lower frequencies, on average, in a turbulence signal, the larger scales are preferentially fixed in place first. However, this is not something that is imposed by the method. As a consequence, highly energetic, high frequency events will be fixed in preference to lower frequency features with less energy. We then applied the method described in Sec. II to the original data and the synthetic data. Variation in the coefficients in Eqs. (7) and (8) as a function of ϑ provides an insight into the difference in the nature of wakes forced by single and multiple scales.

IV. EXPERIMENTAL DATA

The cylinder wake data studied here were obtained in the far wake region behind a 0.02 m diameter cylinder mounted on the center line of a wind tunnel. Measurements were taken with hot wire anemometry on the center line at a distance one hundred diameters downstream of the cylinder using a cross wire oriented to perpendicular to the cylinder. The velocities for the low and high Reynolds number cases were 8.47 m s^{-1} and 25.37 m s^{-1}, respectively, and the corresponding acquisition frequencies were 15 kHz and 85 kHz, respectively, with a turbulence intensity ~5% for both cases.[37] The fractal grid data examined here were obtained by Seoud and Vassilicos[12] in a wind tunnel with a 4.2 m long working section, a 0.212 m^2 cross section, and a background turbulence intensity of 0.4%. Flow velocities were measured by hot wire anemometry with a 1 mm long platinum element of 5 μm diameter at 80 kHz. The fractal grid has four iterations of a square pattern and a blockage ratio of 25%. The effective mesh size, M_{eff},[11] is 26.2 mm and the thickness ratio between the largest square's cross-stream thickness and that of the smallest is 17. The wakes resulting from two different inlet velocities, $U_\infty \in \{7, 16\}$ m s^{-1}, are examined here. Measurements were taken in the decay region where turbulence is homogeneous and isotropic at small scales. The turbulence intensities' downstream of the fractal grids was always less than 10% meaning that Taylor's hypothesis was used to produce a spatial velocity series.

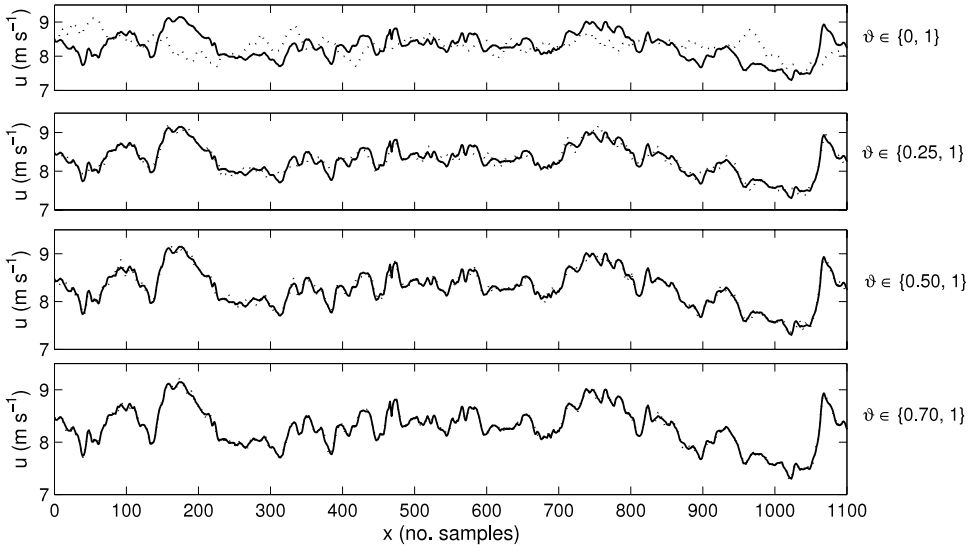

FIG. 2. An example of gradual wavelet reconstruction for our lower *Re* cylinder wake dataset. The original data ($\vartheta = 1$) are shown in black in each panel. The black dotted lines are surrogate series at $\vartheta \in \{0.00, 0.25, 0.50, 0.70\}$ from bottom to top, respectively.

V. RESULTS

Figure 3 examines the robustness of the estimation of the parameters in Eqs. (7) and (8) as a function of r for nine realizations of a synthetic series at a selected value for ϑ for the low Reynolds number, fractal wake case. The different symbols represent the four parameters and the subpanels are for realizations at different ϑ. There is almost no visible deviation in any of the estimated values for any of the parameters at any ϑ across the nine realizations. Thus, a dataset of 3 000 000 values, equating to ~10 000 integral scales, is sufficiently long to permit robust estimation of the parameters in the Fokker-Planck equation for the increments. Based on this result, we reduced the computational time significantly by generating one synthetic dataset for a given ϑ for each original dataset.

Figure 4 shows the evaluation of the terms in Eq. (6) as a function of r. The lack of dependence on ϑ for all coefficients except those included in Eqs. (7) and (8) is clear for both the turbulence data and the synthetic variants, in agreement with other studies.[21,36] It is clear that phase randomization has the greatest impact on the results for d_{21} and d_{22}, where the crosses and pluses equate to zero for all r/l_{em}. This confirms the explanation that it is these terms that contain direct information on the anomalous scaling of the structure functions as a phase randomized variant ($\vartheta = 0$) will be similar in nature to a fractional Brownian motion with any intermittency only remaining by chance.

A further advantage of synthetic data methods is clear: confidence can be placed on the results for d_{21} and d_{22} such that, although the magnitudes are much smaller than d_{20} and d_{11}, they are shown to be significantly different to zero. Hence, while it is understandable based on the relative magnitudes of these coefficients that previous work has focused on d_{20},[21] this study highlights that the linear and quadratic terms are more sensitive markers of turbulence structure.

A. Gradual wavelet reconstruction of d_{20}

Previous work has focused on the derivative of d_{20} with respect to r/l_{em}, termed d_{20}^*[21] because of the linear scaling that can be seen in Fig. 4. The relation between d_{20}^* and ϑ is given in Figure 5. The value for d_{20}^* increases for ϑ in an approximately linear fashion once $\vartheta \geq 0.25$. That is, once 25% of the wavelet energy is fixed in the synthetic data, the equation for the evolution of the increments broadly respects the physics contained in the original data. There is then a linear convergence upon the true result as a function of ϑ and the slope of this scaling, $\frac{d\, d_{20}^*}{d\vartheta}$, for $0.25 \leq \vartheta \leq 0.9$ has the values given in Table I. There is evidence here that not only is d_{20}^* a Reynolds number

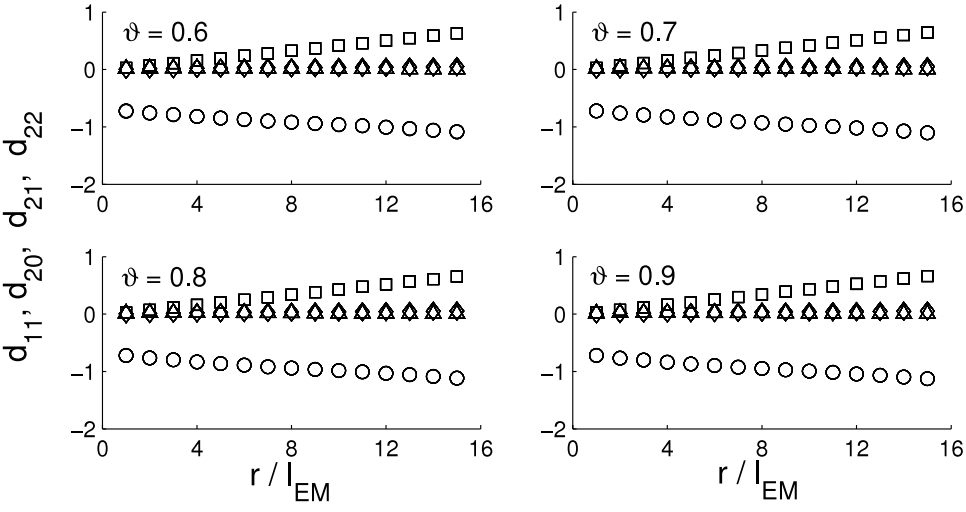

FIG. 3. The scaling of values for d_{11} (circles), d_{20} (squares), d_{21} (diamonds), and d_{22} (triangles) against r/l_{EM} for the low Reynolds number fractal-forced dataset at four values for ϑ. Although barely visible, nine symbols of a given type are plotted at a given r/l_{EM} to confirm precise estimation of these parameters for a synthetic data series generated at a particular ϑ.

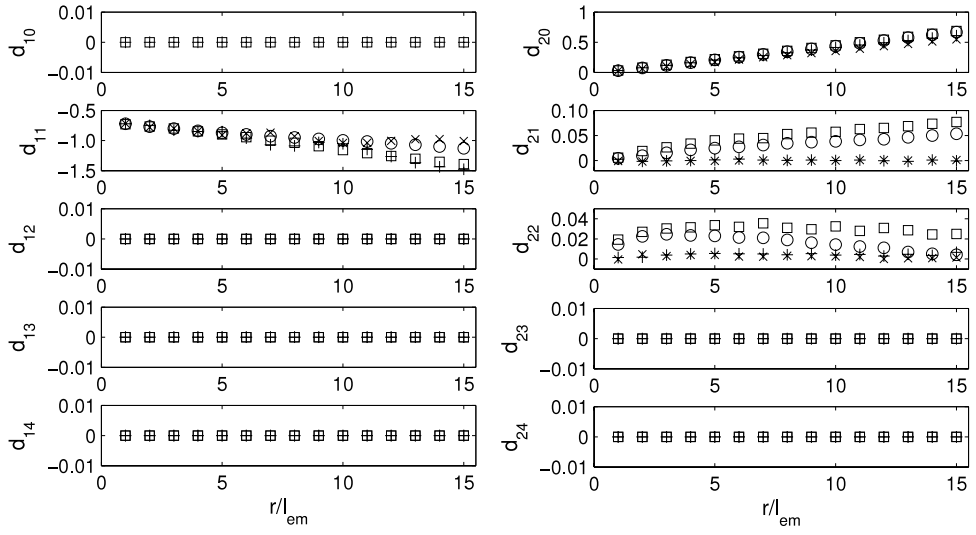

FIG. 4. The scaling of the coefficients obtained from power-law expansions of $D^{(1)}$ and $D^{(2)}$. Black squares are for the low Reynolds number cylinder wake data, and circles are for the low Reynolds number fractal wake data. Surrogates at $\vartheta = 0$ are shown as crosses for the fractal wake and as pluses for the cylinder wake.

independent constant for fractal-forced flows,[21] but also the rate at which fractal-forced flows attain their true value as the nonlinear structure of the turbulence in the inertial regime is imposed is also more constant than for turbulence forced in other ways, which we consider further in Sec. VII. The cylinder wake results do not collapse when the difference in the values for d^*_{20} for the original data is accounted for, as is shown in Fig. 5(b); the high Reynolds number case for the cylinder wake is still different in nature to the other cases, and the low Reynolds number cylinder wake has the highest value for $d\, d^*_{20}/d\vartheta$.

B. Gradual wavelet reconstruction of d_{11}

Figure 4 shows an approximately linear relation between d_{11} and r/l_{em} for $r/l_{em} \geq 3$ and Fig. 6 indicates the gradients of the fits to these data as a function of ϑ, similar to Fig. 5. There is no Reynolds independence for the fractal forced cases for d^*_{11} in Fig. 6(a), in contrast to the results seen

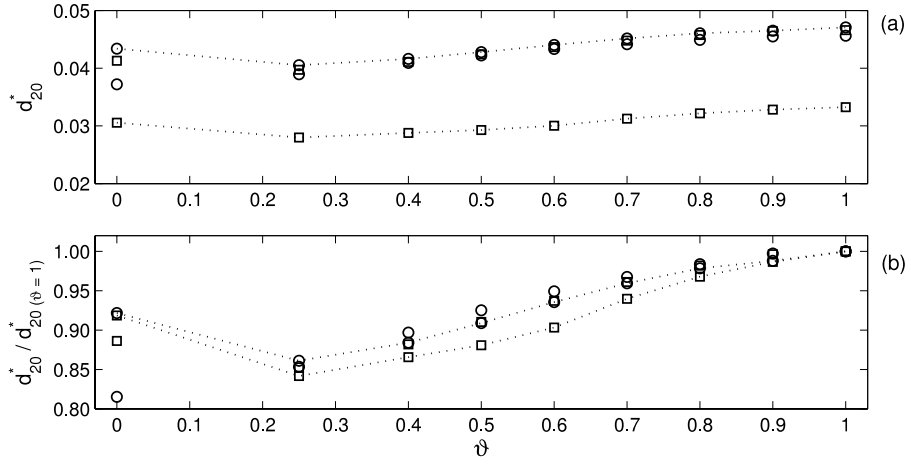

FIG. 5. The relation between ϑ and d^*_{20} for the four wake flows. In the bottom plot, these values are normalized by the result at $\vartheta = 1$. The circles are the fractal-forced wakes and the squares are wakes forced by the cylinder. The high Reynolds number cases are indicated by a dotted line connecting the symbols.

TABLE I. Scaling behavior of d^*_{20}, d^*_{11}, and K_c against ϑ for the four datasets: "wake" is the cylinder wake and "fractal" is the fractal square grid-forced wake.

Re	Flow type	$d\,d^*_{20}/d\vartheta$	$d\,d^*_{11}/d\vartheta$	$d\,K_c/d\vartheta$
Low	Wake	0.0108	−0.0138	0.0109
High	Wake	0.0078	−0.0105	0.0133
Low	Ffractal	0.0101	−0.0085	0.0092
Hhigh	Fractal	0.0099	−0.0137	0.0081

in Fig. 5(a). However, when results are normalized by $d^*_{11(\vartheta=1)}$ in Fig. 6(b), it would appear that all data follow a similar curve, with two important distinctions compared to Fig. 5(b): while the scaling with ϑ appears to occur for $\vartheta \geq 0.25$ for the fractal forced cases, this is true for $\vartheta \geq 0.40$ for the cylinder wakes, and although the two types of wake have a different scaling behavior for $\vartheta = 0.25$ in Fig. 6(b), these are Reynolds number independent and consistent within flow type. That the multi-scale forced wake "locks on" to the scaling relation at a lower ϑ than the cylinder wake data, which indicates that the synthetic increment structure for such a forcing is more "turbulence-like" more readily. This is consistent with the observation that the increment moments for multiscale forced wakes are more similar to homogeneous, isotropic turbulence (HIT) than for single-scale forced flows[20] and is explained in terms of a "space-scale unfolding (SSU) mechanism"[17] in Sec. VII.

C. Gradual wavelet reconstruction of d_{21} and d_{22}

Because the absolute values for d_{21} and d_{22} are much smaller than for d_{11} and d_{20}, their behavior is difficult to discern in Figs. 3 and 4. Figure 7 provides a more complete view than Fig. 4 and it is clear that at $\vartheta = 0$, the values for d_{21} and d_{22} are very close to zero for all cases, which was not the case for d_{20}. Hence, phase randomization can generate values for the constant term in the expansion of the diffusion coefficient that is not dissimilar to the correct values (Fig. 5(b)), but values for the linear and quadratic terms are certainly incorrect. By $\vartheta = 0.5$, the series shown in Fig. 7 contain significant real structure relative to the values for the original data, particularly for the low Reynolds number, fractal-forced case. This clear ability to discriminate between real turbulence and phase-randomized variants for relatively high order terms in the expansion of $D^{(2)}$ demonstrates the precision of the Fokker-Planck approach for studying the increments and also shows how GWR is useful for placing confidence on these values when the absolute values are relatively small.

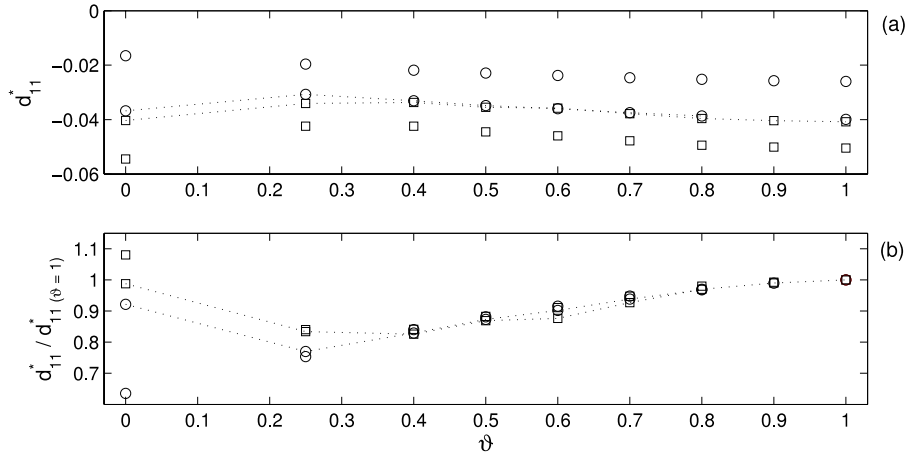

FIG. 6. The relation between ϑ and d^*_{11} for the four wake flows. In the bottom plot, these values are normalized by the result at $\vartheta = 1$. The circles are the fractal-forced wakes and the squares are wakes forced by the cylinder. The high Reynolds number cases are indicated by a dotted line connecting the symbols.

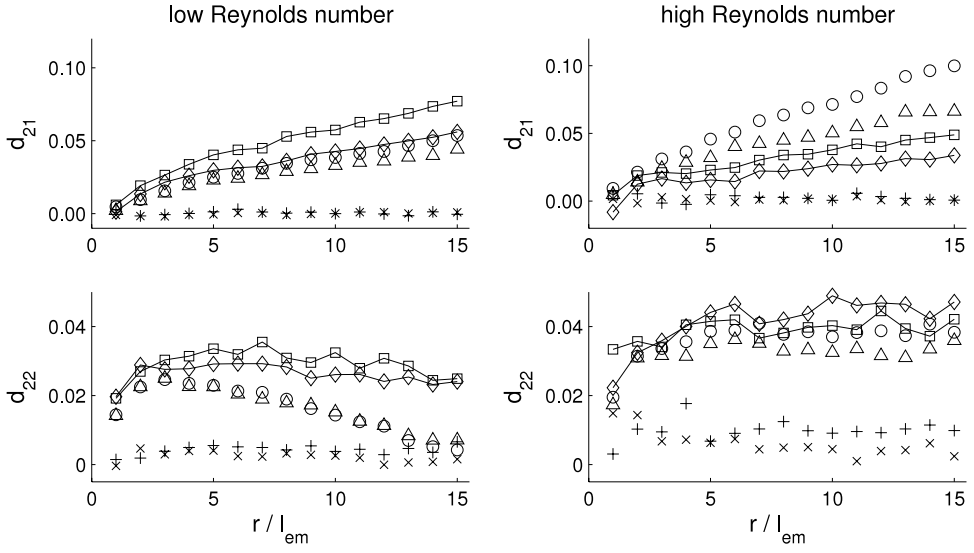

FIG. 7. The scaling of the d_{21} and d_{22} coefficients against r/l_{em} as a function of $\vartheta \in \{0.0, 0.5, 1.0\}$. Squares are the cylinder wake flows and circles are the fractal cases for $\vartheta = 1.0$. Diamonds and triangles are the cylinder and the fractal wake, respectively, at $\vartheta = 0.5$. Values for d_{21} and d_{22} at $\vartheta = 0.0$ are similar to zero and are shown by crosses and pluses for the fractal and single-scale forcings, respectively.

The results for d_{21} scale linearly with r, at least for $r/l_{em} \gtrsim 5$, meaning that a variable $d^*_{21} = d\, d_{21}/dr$ may be formed in an analogous way to d^*_{20}, studied above, and this is plotted in Fig. 8 as a function of ϑ. In contrast, the results for d_{22} generally attain a constant for $r/l_{em} \gtrsim 5$, and this result is also observed in the GWR data at $\vartheta = 0.5$, indicating that there is a scale independence to the quadratic term above a few Taylor scales, which presumably reflects the preferential removal of vortices by viscosity at the smaller scales. Given the different behavior of d_{22}, instead of analyzing $d^*_{22} = d\, d_{22}/dr$, we examine the intercept, d^+_{22}, of the fitted least squares relation between d_{22} and r as a function of ϑ (Fig. 9).

The results shown in Figs. 8 and 9 exhibit no clear dependence on Reynolds number or the nature of the forcing. Figure 8(b) shows a convex convergence on the original value for d^*_{21} that fits all the data over the full range of ϑ, in contrast to the results for d^*_{20} at $\vartheta = 0$ and for d^*_{11} at $\vartheta \in \{0, 0.25\}$. For d^+_{22}, by $\vartheta = 0.6$, all data would appear to have converged on the asymptotic limit with low error (Fig. 9(b)), and this value would appear to be a constant irrespective of forcing or

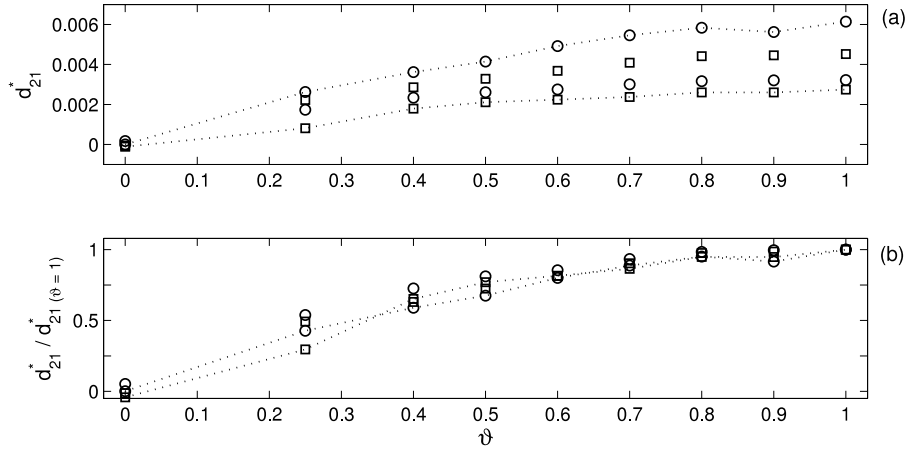

FIG. 8. The relation between ϑ and d^*_{21} for the four wake flows. In the bottom plot, these values are normalized by the result at $\vartheta = 1$. The circles are the fractal-forced wakes and the squares are wakes forced by the cylinder. The high Reynolds number cases are indicated by a dotted line connecting the symbols.

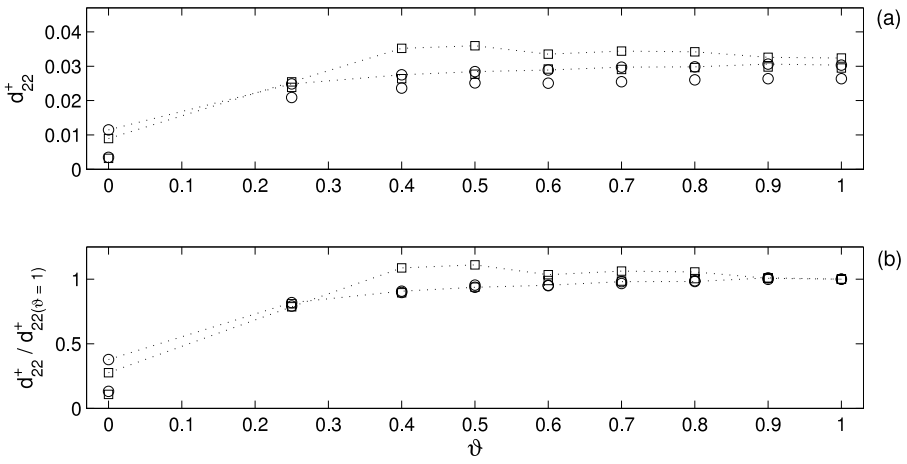

FIG. 9. The relation between ϑ and d^+_{22} for the four wake flows. In the bottom plot, these values are normalized by the result at $\vartheta = 1$. The circles are the fractal-forced wakes and the squares are wakes forced by the cylinder. The high Reynolds number cases are indicated by a dotted line connecting the symbols.

Reynolds number (Fig. 9(a)). In summary, GWR has facilitated an analysis of the linear and the quadratic terms in Eq. (8), and there appears to be a universality in their scaling behavior with ϑ, meaning that the effect of forcing is concentrated on d^*_{20} as suggested previously.[21] However, GWR has shown that phase randomized synthetic data ($\vartheta = 0$) are able to attain the values for d^*_{20} and d^*_{11} (the left-hand side of Fig. 5(a) and Fig. 6(a)) but this is certainly not the case for d^*_{21} and d^*_{22}. Thus, it is with these latter parameters that true turbulence may be most readily distinguished from synthetic variants in a fashion that appears to be forcing and Reynolds number independent. This result may be useful as a test statistic for synthetic inlet turbulence generation schemes, an area that has been recognized as of increasing importance for large-eddy simulations.[47,53]

VI. INTERPRETATION IN TERMS OF THE KOLMOGOROV CAPACITY, K_c

In this section, we study an alternative property of turbulence that may be related to flow topology and increment statistics, the Kolmogorov capacity, K_c.[54] The study of K_c is closely related to the analysis of stochastic signals[55] and the average distance between each zero crossing may be related to the viscous dissipation scale.[56] Early work on the scaling properties of these zero-crossings was undertaken by Kolmogorov[27] and the box counting dimension of the zero-crossings of a fluctuating velocity signal has subsequently been termed the Kolmogorov capacity, K_c.[57] This measures how evenly energy is distributed across wavenumbers in Fourier space[52] and is defined as

$$M_{0c}(r) \sim r^{-K_c}, \tag{13}$$

where r is the increment length and M_{0c} is the minimum number of balls with diameter r needed to cover the zero-crossings of a velocity signal $u(x)$. Hence, $0 \leq K_c \leq 1$ is the box-counting dimension of the set of zero-crossing points on the line.

In contrast to Sec. V, which focus on small-scale intermittency (as we randomized between l_{em} and L), the Kolmogorov capacity will preferentially reflect intermittency at larger scales. This is because excursions from the mean velocity (which on average will lead to a larger spacing of the zero crossings of $u(x)$) will integrate the effect of fluctuations at all scales but will be dominated on average by those at lower wavenumber. To illustrate this, Fig. 10(a) shows a fractional Brownian motion,[58] m_1, with a constant Hölder exponent of $\alpha(t) = 1/3$, i.e., it obeys Kolmogorov's 2/3 law. This may be contrasted with the multifractional Brownian motion,[59] m_2, shown in Fig. 10(b), which also obeys the 2/3 law on average ($\overline{\alpha} = 1/3$), but intermittency is imposed according to $\alpha(t) = 0.33 + 0.15\sin(8\pi t)$. Both time series were generated using a Gaussian random field generation

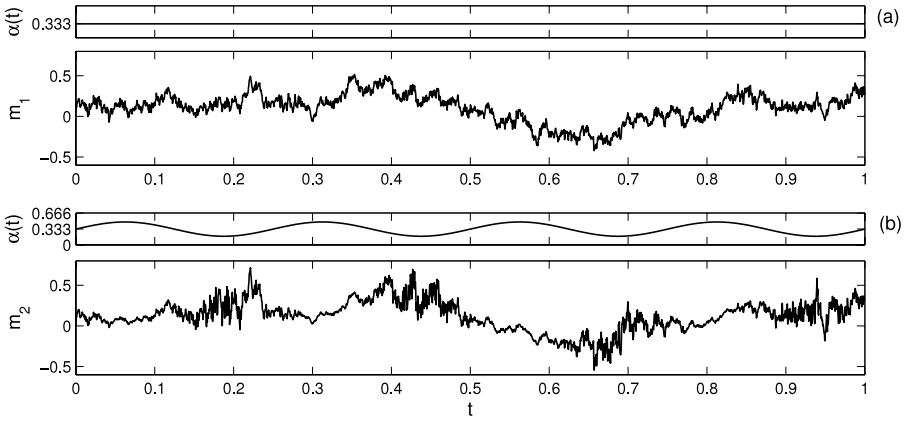

FIG. 10. A fractional Brownian motion (m_1) and a multifractional Brownian motion (m_2) generated from the same random seed. The generating Hölder exponent function, $\alpha(t)$, is shown in each case above the respective stochastic signal [straight line for (a), sine wave for (b)].

algorithm,[60] using the same random seed in each case so that m_1 and m_2 are broadly similar in shape. Values for K_c for these two cases were 0.613 (m_1) and 0.6224 (m_2), highlighting the more intermittent nature of the energy distribution in the latter case.

Figure 11 shows K_c as a function of ϑ for the four wakes, and the values for $dK_c/d\vartheta$ for $\vartheta \geq 0.4$ are given in Table I. Note that the difference between $K_c(\vartheta = 0.25)$ and $K_c(\vartheta = 1.0)$ is approximately 0.07, which is a similar order to the results for m_1 and m_2 from Fig. 10. Hence, the scaling of K_c with ϑ may be related to the recovery of intermittency in the synthetic data once the basic nonlinear structure has been imposed at $\vartheta = 0.25$. There are some similarities and some differences with the results for d^*_{20}. In terms of the similarities,

- the unconstrained randomization at $\vartheta = 0$ can yield feasible values for K_c; a higher value of ϑ is needed to "lock" the properties of the synthetic data to the original;
- this "locking" value for ϑ is lower for the multiscale forced cases than the cylinder wakes ($\vartheta = 0.25$ as opposed to $\vartheta = 0.40$);
- there is then an approximately linear scaling, and the values for $dK_c/d\vartheta$ are similar for the two fractal-forced cases with the cylinder wakes exhibiting a stronger Reynolds dependence to the rate of convergence on the original K_c.

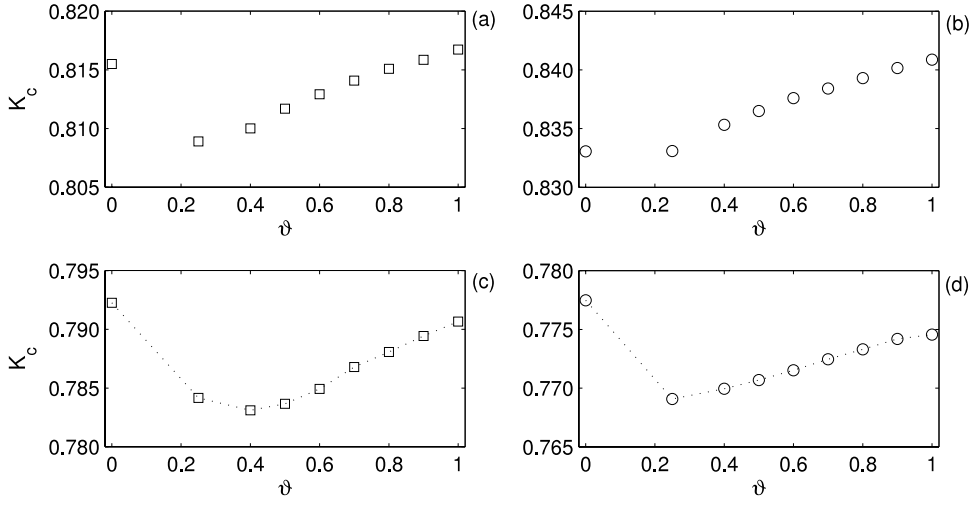

FIG. 11. The relation between ϑ and the Kolmogorov capacity for the four wake flows. The circles are the fractal-forced wakes and the squares are wakes forced by the cylinder. The high Reynolds number cases are indicated by a dotted line connecting the symbols.

An obvious difference is that while the high Reynolds number cylinder wake has a much lower value for $d\,d^*_{20}/d\vartheta$ than the other datasets, it has the highest for $d\,K_c/d\vartheta$. Furthermore, $d\,K_c/d\vartheta$ clearly partitions the cylinder wakes and multiscale-forced wakes, with the latter having lower values, indicating that the relevant nonlinear structure to attain K_c is imposed earlier with the multi-scale forcing. Hence, the nature of the forcing would appear clearly distinguished in K_c with higher values for single scale forcings, while in the scaling region, the single-scale forcing contrasts with that at multiple scales by exhibiting greater Reynolds dependence.

VII. DISCUSSION

A. A space-scale unfolding mechanism for multiscale forcing

Recent numerical simulations of turbulence decay behind otherwise similar regular and fractal grids have shown that the former generates a peak average turbulence intensity more than three times higher than the fractal case and, consistent with this, a much higher peak average pressure drop.[17] However, while the average turbulence intensity $\langle u'^2\rangle/U_0^2$ has decayed to less than 1% by ten effective mesh lengths for the regular grid, it is still a few percent at fifty effective mesh lengths for the fractal grid, with a concomitant reduction in the rate of pressure recovery.[17] These authors explain this in terms of a space-scale unfolding mechanism (SSU). In effect, the turbulence generated by the fractal grid is distributed along the longitudinal direction, reducing the peak in turbulence intensity because wakes generated by different sized elements interact at different distances' downstream. Diffusivity increases as a consequence of this mechanism[14] because, from a Lagrangian perspective, a fluid element may potentially move from one wake to a larger one as it progresses downstream, with each larger wake having a larger eddy turnover time. In the theory of decaying homogeneous turbulence, it is usually considered that[61]

$$\epsilon = C_\epsilon \frac{\sigma_u^3}{L}, \tag{14}$$

where σ_u is the standard deviation of the velocity, L is the integral scale, and C_ϵ is a constant that is potentially a function of boundary conditions. Note that this is a Reynolds number independent result, hence, as Reynolds number increases, L/λ increases,where λ is the Taylor scale, as more scales are excited. In contrast, the wakes for fractal space filling grids have been shown to obey $L/\lambda = (C_\epsilon/15)Re_\lambda$, with an additional dependence between C_ϵ and the grid Reynolds number and an absence of a Richardson-Kolmogorov cascade.[62] This process is complicated by transverse turbulence transport[14,63] as explained from a Lagrangian perspective, above.

This SSU mechanism can also be used to interpret the results presented here concerning the behavior of $d\,K_c/d\vartheta$ and $d\,d^*_{20}/d\vartheta$. The intermittency for multi-scale generated wakes is higher than for single-scale generation mechanisms.[20,64] For a single scale forcing that is $\sim L$, the scales between l_{em} and L are exhibiting decay in the Richardson-Kolmogorov sense. For multi-scale forced flow, there is a response to direct forcing at scales smaller than L, enhancing large-scale intermittency. Thus, from the perspective of GWR, at $\vartheta \sim 0.25$, where phase randomization is constrained, but relatively little nonlinear structure has yet to be imposed, the fixed wavelet coefficients for the single-scale forcing will essentially all be large scale coefficients. In contrast, enhanced intermittency means that there is an increased probability that the wavelet coefficients fixed for the multiscale forcing reflect both the energy cascade and the intermittency. Hence, features pertinent to the definition of K_c are fixed at a lower ϑ in this case. Thus, the values for $d\,K_c/d\vartheta$ are lower for the multiscale forced wakes. Related to this is the lack of Reynolds number dependence for $d\,d^*_{20}/d\vartheta$ for the multiscale forcing: the vortex structure imposed by SSU dominates Reynolds number effects for the multiscale forcing, explaining why $d\,d^*_{20}/d\vartheta \sim 0.01$ for both Re.

B. Implications of the results for reduced order modeling

Reduced order modeling of turbulent flows using dimensional reduction methods such as Proper Orthogonal Decomposition (POD)[65,66] extends back to the 1980s.[41] Having defined an

acceptable number of modes, a Galerkin system of evolution equations is written for the modes in terms of advective and dissipative terms, with the latter modeled to prevent excessive energy build-up (some form of cascade is required). Approaches are inspired by an eddy-viscosity approach,[41] with more advanced closures incorporating linear approximations to the nonlinear terms[67] or nonlinear interactions directly,[68] and comparative analyses demonstrating the utility of these more advanced formulations.[42] While dyadic wavelet modes are locally correlated at singularities (providing the basis for multifractal methods[25]), they provide an approximately orthogonal or orthonormal basis that is also conditioned on frequency. Thus, while POD enforces orthogonality but any scale separation is implicit, wavelets enforce the latter. Applying GWR at a given choice of ϑ means some $w_{j,k}$ are fixed but the randomisation of others at a given scale, j, acts to alter singularity structure while preserving energy at that j. Consequently, employing GWR in the context of a POD and studying how the closure to the Galerkin system responds would be a novel way to gain an insight into reduced order modeling methods.

In addition, it has been shown previously how the PDF method used in this study can be used to simulate stochastic systems with a given (multifractal) structure.[39] Hence, a modified Galerkin system based on a stochastic model would be an alternative nonlinear closure. Our results imply that for $r/l_{em} > 5$, a constant value of d_{22} is appropriate that should be a weak function of Reynolds number. In contrast, d_{11} and d_{21} can be modeled as linear functions of scale, $d_{11} \sim -0.04 r/l_{em}$, $d_{21} \sim 0.004 r/l_{em}$, with the results for the latter (left-hand side of Fig. 6(b)) implying that enough POD modes are needed to ensure that quality results are a consequence of accurate modeling, not random variation in the residual modeling. A similar point applies to the modeling of d_{20}, where a Reynolds number dependence exists for the cylinder wakes and not the multiscale forcing. This latter result implies that with some knowledge of the large scale forcing, it may be possible to tune the closure appropriately. However, the results for K_c highlight that information on the nature of the forcing exists and a more complex model would be needed to couple large and small scales.

VIII. CONCLUSION

The definition of the parameter ϑ in GWR has been modified in this study to consider only the energy between the integral and Markov lengths. Based on this, four wake datasets have been randomized for eight choices of ϑ and the properties of the increment distributions as a function of scale, r, compared to the original data. Consistent with previous work that identified a Reynolds number independence for fractal wakes for the value for d^*_{20}, we have found that the scaling for this term as a function of ϑ is also Reynolds number independent. Any such dependence for d^*_{11} only occurred at low ϑ. The result for $d\, d^*_{20}/d\vartheta$, which indicates a clear difference in behavior for the single- and multi-scale forcing, is related to smaller scale structure. We also studied the scaling of the Kolmogorov capacity with ϑ, $d\, K_c/d\vartheta$, which concerns larger scale intermittency in the flow. This scaling for K_c was lower for the multiscale forced cases and these results may be interpreted with respect to the "space-scale unfolding mechanism," proposed recently to explain differences in turbulence structure between single- and multiscale-forced wakes.[17]

The use of GWR has provided confidence in the analysis of the values for d_{21} and d_{22} as a function of r/l_{em}. As with d_{20} and d_{11}, with d_{21}, there is a linear dependence on scale, meaning that $d^*_{21} = d\, d_{21}/dr/l_{em}$ can be studied as a function of ϑ and shown to follow a similar curve irrespective of flow type or Reynolds number (Fig. 8(b)). For d_{22}, an asymptotic value, d^+_{22}, appears to be obtained at some r/l_{em} for the majority of the data, and this value is a constant of ~0.03 for all cases and is preserved with high accuracy for $\vartheta \geq 0.6$. While the values for d^*_{21} and d^+_{22} exhibit a similar scaling with ϑ for all cases, it is these values that are critical for discriminating between real and synthetic turbulence time series because of their connection to anomalous scaling.

Values for d^*_{21} and d^+_{22} for high ϑ are very different to those for $\vartheta = 0.0$. In contrast, the phase randomization that occurs at $\vartheta = 0.0$ means that values for d^*_{11}, d^*_{20}, and K_c may be a similar magnitude as the original data. For these cases, a higher choice of $\vartheta = 0.25$ or $\vartheta = 0.4$ is needed to constrain the variation in these parameters such that they then converge on the original data in a stable way. Hence, feasible values for d_{11} and d_{20} can arise by chance in a phase randomization. That

this is not the case for d_{21}^{*} and d_{22}^{+} and that the results for these parameters are similar irrespective of forcing type and Reynolds number make them a more useful means for defining true turbulence and, therefore, evaluating synthetic turbulence generation algorithms.

ACKNOWLEDGMENTS

We wish to thank the Mathematical Institute at Imperial College for hosting a meeting where this work was initiated, as well as the kind support of Richard Seoud and Christos Vassilicos, who provided us with the fractal square grid data studied here.

APPENDIX: WAVELET TRANSFORMS

A continuous wavelet transform[25,69,70] yields wavelet coefficients, $w(j,k)$ of a time series $x(t)$ at a scale, $j > 0$, and a position, $k \in \Re$, from a convolution of the time series with a wavelet function, ψ, whose integral is zero and whose square integrates to unity,

$$w(j,k) = \frac{1}{\sqrt{j}} \int_{-\infty}^{+\infty} x(t)\psi^{*}(t - k/j)\, dt, \tag{A1}$$

where $*$ is the complex conjugate. An additional admissibility constraint on the form of the wavelet function, which permits a reconstruction of the original signal, is that its Fourier transform

$$\Psi(f) \equiv \int_{-\infty}^{+\infty} \psi(t) e^{-2\pi f t i}\, dt \tag{A2}$$

is such that $0 < C_{\psi} < \infty$, where

$$C_{\psi} \equiv \int_{0}^{\infty} \frac{|\psi(f)|^2}{f}\, df. \tag{A3}$$

As such, it follows that

$$\int_{-\infty}^{+\infty} x^2(t)\, dt = \frac{1}{C_{\psi}} \int_{0}^{\infty} \left[\int_{-\infty}^{+\infty} w^2(j,k)\, dt \right] \frac{dj}{j^2}, \tag{A4}$$

which shows that $w^2(j,k)/j^2$ is the energy function of the signal decomposed over different scales and positions, explaining the definition of ϑ in the main text.

Because surrogate data algorithms involve a deconstruction of an original signal, a manipulation, and a subsequent reconstruction, the integral formulation for the inverse transform in (A1) makes reconstruction using the continuous transform problematic. The DWT is based on a hierarchical set of filtering operations, aiding accurate reconstruction. A DWT of a time series sampled at $N = 2^J$ points can be formulated over the dyadic scales 2^j, $j = 1, \ldots, J$ using a filter bank of low and high pass quadrature mirror filters of even filter width. Although the DWT gives a compact representation of the signal, it has the following limitations:[48]

- circularly shifting $x(t)$ by some amount cannot be represented by applying a similar shift to the $w_{j,k}$;
- because the wavelet filters are not zero phase, aligning the coefficients with the original time series is not straightforward;
- circularly shifting $x(t)$, taking the discrete transform, and determining the wavelet power spectrum do not necessarily return the same wavelet spectrum as for $x(t)$.

The first and last points are particularly important for surrogate generation as estimations of the local energy content of the signal should be robust to a rotation of the data and preservation of linear features of the original data in the surrogates is important. Consequently, the wavelet power spectrum should retain a simple relation to the Fourier power spectrum.

The translation invariant, stationary, or MODWT is an undecimated variant of the discrete transform that avoids some of the above issues. Effectively, a discrete transform is undertaken for all N circular rotations of $x(t)$. For any given minimum rotation of $x(t)$, most coefficients will

be identical to those at the previous iteration meaning that the computation of the MODWT is $O(N \log_2 N)$ and not $O(N^2)$.[71]

Defining the filter width at scale j as $L_j \equiv (2^j - 1)(L - 1) + 1$, the jth level MODWT high and low pass filters are given as

$$\tilde{h}_{j,l} \equiv h_{j,l}/2^{j/2},$$
$$\tilde{g}_{j,l} \equiv g_{j,l}/2^{j/2}. \tag{A5}$$

These MODWT filters are related to those used in the DWT except for a rescaling to account for the lack of downsampling. Hence, the MODWT wavelet and approximation coefficients are given as[48]

$$w_{j,k} \equiv \sum_{l=0}^{L_i-1} \tilde{h}_{j,l} x_{k-l \bmod N},$$
$$A_{j,k} \equiv \sum_{l=0}^{L_i-1} \tilde{g}_{j,l} x_{k-l \bmod N}. \tag{A6}$$

[1] A. N. Kolmogorov, "The local structure of turbulence in incompressible viscous fluid for very large Reynolds numbers," Dokl. Akad. Nauk SSSR **30**, 299–303 (1941).
[2] A. N. Kolmogorov, "A refinement of previous hypotheses concerning the local structure of turbulence in a viscous, incompressible fluid at high Reynolds number," J. Fluid Mech. **13**, 82–85 (1962).
[3] U. Frisch, P. L. Sulem, and M. Nelkin, "Simple dynamical model of intermittent fully developed turbulence," J. Fluid Mech. **87**, 719–736 (1978).
[4] C. Meneveau and K. Sreenivasan, "The multifractal nature of turbulent energy-dissipation," J. Fluid Mech. **224**, 429–484 (1991).
[5] Z. S. She and E. Leveque, "Universal scaling laws in fully developed turbulence," Phys. Rev. Lett. **72**, 336–339 (1994).
[6] M. Dowker and K. Ohkitani, "Intermittency and local Reynolds number in Navier–Stokes turbulence: A cross-over scale in the Caffarelli–Kohn–Nirenberg integral," Phys. Fluids **24**, 115112 (2012).
[7] N. Mazellier and J. C. Vassilicos, "The turbulence dissipation constant is not universal because of its universal dependence on large-scale flow topology," Phys. Fluids **20**, 015101 (2008).
[8] P. K. Yeung and J. G. Brasseur, "The response of isotropic turbulence to isotropic and anisotropic forcing at the large scales," Phys. Fluids A **3**, 884–897 (1991).
[9] K. Ohkitani and S. Kida, "Triad interactions in forced turbulence," Phys. Fluids A **4**, 794–802 (1992).
[10] A. K. Kuczaj, B. J. Geurts, and W. D. McComb, "Nonlocal modulation of the energy cascade in broadband-forced turbulence," Phys. Rev. E **74**, 016306 (2006).
[11] D. Hurst and J. C. Vassilicos, "Scalings and decay of fractal-generated turbulence," Phys. Fluids **19**, 035103 (2007).
[12] R. E. Seoud and J. C. Vassilicos, "Dissipation and decay of fractal-generated turbulence," Phys. Fluids **19**, 105108 (2007).
[13] P. C. Valente and J. C. Vassilicos, "Universal dissipation scaling for nonequilibrium turbulence," Phys. Rev. Lett. **108**, 214503 (2012).
[14] K. Nagata, Y. Sakai, T. Inaba, H. Suzuki, O. Terashima, and H. Suzuki, "Turbulence structure and turbulence kinetic energy transport in multiscale/fractal-generated turbulence," Phys. Fluids **25**, 065102 (2013).
[15] W. K. George, "The decay of homogeneous isotropic turbulence," Phys. Fluids A **4**, 1492 (1992).
[16] W. K. George and H. Wang, "The exponential decay of homogeneous isotropic turbulence," Phys. Fluids **21**, 025108 (2009).
[17] S. Laizet and J. C. Vassilicos, "Fractal space-scale unfolding mechanism for energy-efficient turbulent mixing," Phys. Rev. E **86**, 046302 (2012).
[18] H. Suzuki, K. Nagata, Y. Sakai, T. Hayase, Y. Hasegawa, and T. Ushijima, "Direct numerical simulation of fractal-generated turbulence," Fluid Dyn. Res. **45**, 061409 (2013).
[19] F. C. G. A. Nicolleau, S. M. M. Salim, and A. F. Nowakowski, "Experimental study of a turbulent pipe flow through a fractal plate," J. Turbul. **12**, N44 (2011).
[20] C. J. Keylock, K. Nishimura, M. Nemoto, and Y. Ito, "The flow structure in the wake of a fractal fence and the absence of an 'inertial regime'," Environ. Fluid Mech. **12**, 227–250 (2012).
[21] R. Stresing, J. Peinke, S. Seoud, and J. Vassilicos, "Defining a new class of turbulent flows," Phys. Rev. Lett. **104**, 194501 (2010).
[22] T. von Karman and L. Howarth, "On the statistical theory of turbulence," Proc. R. Soc. London, Ser. A **164**, 192 (1938).
[23] C. J. Keylock, "Characterizing the structure of nonlinear systems using gradual wavelet reconstruction," Nonlinear Processes Geophys. **17**, 615–632 (2010).
[24] U. Frisch and G. Parisi, "The singularity structure of fully developed turbulence," in *Turbulence and Predictability in Geophysical Fluid Dynamics and Climate Dynamics*, edited by M. Ghil, R. Benzi, and G. Parisi (North Holland, 1985), pp. 84–88.
[25] J. F. Muzy, E. Bacry, and A. Arnéodo, "Wavelets and multifractal formalism for singular signals: Application to turbulence data," Phys. Rev. Lett. **67**, 3515–3518 (1991).
[26] S. Jaffard, "Multifractal formalism for functions. 1. Results valid for all functions," SIAM J. Math. Anal. **28**, 944–970 (1997).
[27] A. N. Kolmogorov, "A new metric invariant of transitive dynamical systems and automorphisms in Lebesgue spaces," Dokl. Akad. Nauk SSSR **119**, 861–864 (1958).

[28] R. Friedrich and J. Peinke, "Description of the turbulent cascade by a Fokker-Planck equation," Phys. Rev. Lett. **78**, 863 (1997).
[29] C. Renner, J. Peinke, and R. Friedrich, "Markov properties of small-scale turbulence," J. Fluid Mech. **433**, 383–409 (2001).
[30] B. Dhruva, Y. Tsuji, and K. R. Sreenivasan, "Transverse structure functions in high-Reynolds-number turbulence," Phys. Rev. E **56**, R4928–R4930 (1997).
[31] R. A. Antonia and B. R. Pearson, "Low-order velocity structure functions in relatively high Reynolds number turbulence," Europhys. Lett. **48**, 163–169 (1999).
[32] J. Herweijter and W. Van der Water, "Transverse structure functions of turbulence," in *Advances in Turbulence*, edited by V. R. Benzi (Kluwer, New York, 1995), pp. 210–216.
[33] H. Kahalerras, Y. Malecot, and Y. Gagne, "Transverse velocity structure function in developed turbulence," in *Advances in Turbulence VI*, edited by S. Gavrilakis, L. Michiels, and P. A. Monkewitz (Kluwer, New York, 1996), pp. 235–238.
[34] G. P. Romano and R. A. Antonia, "Longitudinal and transverse structure functions in a turbulent round jet: Effect of initial conditions and Reynolds number," J. Fluid Mech. **436**, 231–248 (2001).
[35] R. Camussi and R. Benzi, "Hierarchy of transverse structure functions," Phys. Fluids **9**, 257–259 (1997).
[36] C. Renner, J. Peinke, R. Friedrich, O. Chanal, and B. Chabaud, "Universality of small scale turbulence," Phys. Rev. Lett. **89**, 124502 (2002).
[37] S. Lück, C. Renner, J. Peinke, and R. Friedrich, "The Markov-Einstein coherence length-A new meaning for the Taylor length in turbulence," Phys. Lett. A **359**, 335–338 (2006).
[38] H. Risken, *The Fokker–Planck Equation* (Springer, 1984).
[39] A. P. Nawroth and J. Peinke, "Multiscale reconstruction of time series," Phys. Lett. A **360**, 234 (2006).
[40] A. Arneodo, S. Manneville, J. F. Muzy, and S. G. Roux, "Revealing a lognormal cascading process in turbulent velocity statistics with wavelet analysis," Philos. Trans. R. Soc. London, ser. A **357**, 2415–2438 (1999).
[41] N. Aubry, P. Holmes, J. L. Lumley, and E. Stone, "The dynamics of coherent structures in the wall region of a turbulent boundary layer," J. Fluid Mech. **192**, 115–173 (1988).
[42] J. Östh, B. R. Noack, S. Krajnovic, D. Barros, and J. Borée, "On the need for a nonlinear subscale turbulence term in POD models as exemplified for a high Reynolds number flow over an Ahmed body," J. Fluid Mech. **747**, 518–544 (2014).
[43] J. Theiler, S. Eubank, A. Longtin, B. Galdrikian, and J. Farmer, "Testing for nonlinearity in time-series: The method of surrogate data," Physica D **58**, 77–94 (1992).
[44] T. Schreiber and A. Schmitz, "Improved surrogate data for nonlinearity tests," Phys. Rev. Lett. **77**, 635–638 (1996).
[45] V. Nikora, D. Goring, and R. Camussi, "Intermittency and interrelationships between turbulence scaling exponents: Phase-randomization tests," Phys. Fluids **13**, 1404–1414 (2001).
[46] C. J. Keylock, "A resampling method for generating synthetic hydrological time series with preservation of cross-correlative structure and higher order properties," Water Resour. Res. **48**, W12521, doi: 10.1029/2012WR011923 (2012).
[47] C. J. Keylock, T. E. Tokyay, and G. Constantinescu, "A method for characterising the sensitivity of turbulent flow fields to the structure of inlet turbulence," J. Turbul. **12**, N45 (2011).
[48] D. B. Percival and A. T. Walden, *Wavelet Methods for Times Series Analysis* (Cambridge University Press, Cambridge, UK, 2000).
[49] C. J. Keylock, "Constrained surrogate time series with preservation of the mean and variance structure," Phys. Rev. E **73**, 036707 (2006).
[50] C. J. Keylock, "A wavelet-based method for surrogate data generation," Physica D **225**, 219–228 (2007).
[51] D. L. Donoho and I. Johnstone, "Ideal spatial adaptation by wavelet shrinkage," Biometrika **81**, 425–455 (1994).
[52] N. K.-R. Kevlahan and J. C. Vassilicos, "The space and scale dependencies of the self-similar structure of turbulence," Proc. R. Soc. London, ser. A **447**, 341–363 (1994).
[53] G. Tabor and M. H. Baba-Ahmadi, "Inlet conditions for large eddy simulations: A review," Comput. Fluids **39**, 553–567 (2010).
[54] F. Nicolleau and J. C. Vassilicos, "Wavelets for the study of intermittency and its topology," Philos. Trans. R. Soc. London, Ser. A **357**, 2439–2457 (1999).
[55] S. O. Rice, Bell Syst. Tech. J. **24**, 46–156 (1945).
[56] K. R. Sreenivasan, A. Prabhu, and R. Narasimha, "Zero-crossings in turbulent signals," J. Fluid Mech. **137**, 251–272 (1983).
[57] J. C. Vassilicos and J. C. R. Hunt, "Fractal dimensions and spectra of interfaces with application to turbulence," Proc. R. Soc. London, ser. A **435**, 505–534 (1991).
[58] B. Mandelbrot and J. W. van Ness, "Fractional Brownian motions, fractional noises and applications," SIAM Rev. **10**, 422–437 (1968).
[59] R. Peltier and J. Lévy Véhel, "Multifractional Brownian motion: Definition and preliminary results," Tech. Report No. 2645, INRIA, 1995.
[60] G. Chan and A. T. A. Wood, "Simulation of stationary Gaussian vector fields," Stat. Comput. **9**, 265–268 (1999).
[61] G. K. Batchelor, *The Theory of Homogeneous Turbulence* (Cambridge University Press, 1953).
[62] N. Mazellier and J. C. Vassilicos, "Turbulence without Richardson–Kolmogorov cascade," Phys. Fluids **22**, 075101 (2010).
[63] P. C. Valente and J. C. Vassilicos, "The decay of turbulence generated by a class of multiscale grids," J. Fluid Mech. **687**, 300–340 (2011).
[64] B. Mazzi and J. C. Vassilicos, "Fractal-generated turbulence," J. Fluid Mech. **502**, 65–87 (2004).
[65] G. Berkooz, P. Holmes, and J. L. Lumley, "The proper orthogonal decomposition in the analysis of turbulent flows," Ann. Rev. Fluid Mech. **25**, 539–575 (1993).
[66] J. H. Citriniti and W. K. George, "Reconstruction of the global velocity field in the axisymmetric mixing layer utilizing the proper orthogonal decomposition," J. Fluid Mech. **418**, 137–166 (2000).
[67] M. Balajewicz, E. H. Dowell, and B. R. Noack, "Low-dimensional modelling of high-Reynolds-number shear flows incorporating constraints from the Navier–Stokes equation," J. Fluid Mech. **729**, 285–308 (2013).
[68] B. R. Noack, M. Schlegel, B. Ahlborn, G. Mutschke, M. Morzyński, P. Comte, and G. Tadmor, "A finite-time thermodynamics of unsteady fluid flows," J. Non-Equilib. Thermodyn. **33**, 103–148 (2008).

[69] M. Farge, "Wavelet transforms and their application to turbulence," Ann. Rev. Fluid Mech. **24**, 395–457 (1992).
[70] R. Camussi and G. Guj, "Orthonormal wavelet decomposition of turbulent flows: Intermittency and coherent structures," J. Fluid Mech. **348**, 177–199 (1997).
[71] J. Liang and T. W. Parks, "A translation-invariant wavelet representation algorithm with applications," IEEE Trans. Signal Process. **44**, 225–232 (1996).